Available online at www.sciencedirect.com
SCIENCE DIRECT®
International Journal of Thermal Sciences 44 (2005) 903–911
International Journal of Thermal Sciences
www.elsevier.com/locate/ijts

Thermodynamic analysis of a PEM fuel cell power system

M.M. Hussain [a], J.J. Baschuk [a], X. Li [a], I. Dincer [b,*]

[a] *Department of Mechanical Engineering, University of Waterloo, Waterloo, Ontario N2L 3G1, Canada*
[b] *Faculty of Engineering and Applied Science, University of Ontario Institute of Technology, Oshawa, Ontario L1H 7K4, Canada*

Received 15 October 2004; received in revised form 17 February 2005; accepted 21 February 2005

Available online 9 April 2005

Abstract

This study deals with the thermodynamic modeling of a polymer electrolyte membrane (PEM) fuel cell power system for transportation applications. The PEM fuel cell performance model developed previously by two of the authors is incorporated into the present model. The analysis includes the operation of all the components in the system, which consists of two major modules: PEM fuel cell stack module and system module and a cooling pump. System module includes air compressor, heat exchanger, humidifier and a cooling loop. A parametric study is performed to examine the effect of varying operating conditions (e.g., temperature pressure and air stoichiometry) on the energy and exergy efficiencies of the system. Further, thermodynamic irreversibilities in each component of the system are determined. It is found that, with the increase of external load (current density), the difference between the gross stack power and net system power increases. The largest irreversibility rate occurs in the fuel cell stack. Thus, minimization of irreversibility rate in the fuel cell stack is essential to enhance the performance of the system, which in turn reduces the cost and helps in commercialization of fuel cell power system in transportation applications.

Keywords: Efficiency; Energy and exergy analysis; Fuel cell; Power system; Thermodynamic aspects

1. Introduction

Automobiles using fossil fuel are the major source of harmful air pollutants. Automobiles contribute significantly to the growing environmental concerns such as greenhouse effect, regional acidification and climate change. In addition to these environmental concerns, depletion of fossil fuel reserves and increasing oil prices have generated the need for alternative fuels and energy conversion technologies with minimum environmental impact which can provide energy security, economic growth and sustainable development.

The energy conversion technology which receives considerable attention recently is the proton exchange membrane (PEM) fuel cell, a potential replacement for the conventional internal combustion engine (ICE) in transportation applications. PEM fuel cell is an electrochemical energy conversion device, which converts the chemical energy of hydrogen and oxygen directly and efficiently into electrical energy, with waste heat and liquid water as by-products.

A PEM fuel cell powered automobiles using hydrogen offer several advantages, such as energy efficient and environmentally benign low temperature operation, quick start-up, compatible with renewable energy sources and can obtain a power density competitive with the internal combustion engine [1]. However, the major barriers which are hindering the commercialization of PEM fuel cell powered automobiles are cost and hydrogen infrastructure. One of the means of reducing the cost of PEM fuel cell powered automobile is by improving the performance of PEM fuel cell itself. A proven method of enhancing the performance of energy systems is thermodynamic second law analysis or exergy analysis [2], which is considered to be a primary tool in addressing the impact of energy resource utilization on the environment [3].

In contrast to various studies on exergy analysis of high temperature solid oxide fuel cell for stationary power gener-

* Corresponding author.
E-mail address: ibrahim.dincer@uoit.ca (I. Dincer).

1290-0729/$ – see front matter
doi:10.1016/j.ijthermalsci.2005.02.009

Nomenclature

A_{cell}	cell area	m^2
C_{H_2}	concentration of H_2 at the electrode backing/catalyst layer interface	$mole \cdot m^{-3}$
C_{O_2}	concentration of O_2 at the electrode backing/catalyst layer interface	$mole \cdot m^{-3}$
E	voltage	V
E_r	reversible voltage	V
E_{irr}	irreversible voltage	V
ex	exergy	$J \cdot mole^{-1}$
h	enthalpy	$J \cdot mole^{-1}$
I	current density	$A \cdot m^{-2}$
$\dot{I}$	irreversibility rate	W
$\dot{N}$	molar flow rate	$mole \cdot s^{-1}$
n_{fc}	number of fuel cell in the stack	
$\dot{Q}$	rate of heat lost	W
s	entropy	$J \cdot mole^{-1} \cdot K^{-1}$
S	stoichiometry	
T	temperature	K
V	cell potential	V
$\dot{W}$	power	W
x	mole fraction	

Greek letters

η^a_{act}	anode activation overpotential	V
η^c_{act}	cathode activation overpotential	V
η_{act}	activation overpotential	V
η^a_{bp}	ohmic overpotential of the anode bipolar plate	V
η^c_{bp}	ohmic overpotential of the cathode bipolar plate	V
η^a_{con}	anode concentration overpotential	V
η^c_{con}	cathode concentration overpotential	V
η_{con}	concentration overpotential	V
η^a_e	ohmic losses of the anode electrode backing layer	V
η^c_e	ohmic losses of the cathode electrode backing layer	V
η_{ohmic}	ohmic overpotential	V
η_m	polymer electrolyte membrane overpotential	V
η_{system}	system energy efficiency	%
μ	chemical potential	$J \cdot mole^{-1}$
ψ_{system}	system exergy efficiency	%

Subscripts

ac	air compressor
ch	chemical
cp	cooling pump
ke	kinetic energy
pe	potential energy
rf	radiator fan
tm	thermomechanical
00	unrestricted restricted state
0	restricted state
1,9	thermodynamic states

ation applications, e.g., [2–8] there are only a few studies on exergy analysis that were performed for low temperature PEM fuel cell for transportation applications. Cownden et al. [9] performed exergy analysis of hydrogen fuel cell power system for bus transportation. Their work showed the usefulness of thermodynamic analysis in determining the irreversibilities in different system components, but did not rigorously address the operating characteristics of PEM fuel cell which helps in minimizing irreversibilities and maximizing the performance of the system. Recently, Kazim [10] has conducted exergy analysis of a PEM fuel cell at specified operating voltages of 0.5 and 0.6 V. Exergy efficiency of the PEM fuel cell at different operating conditions were reported; however, the second law characteristic such as irreversibility within the cell was not evaluated since the analysis was performed at specified operating voltages. Additionally, the auxiliary components or balance-of-plant were not included in his study.

Thus, in the present study, thermodynamic analysis of a PEM fuel cell power system for light-duty fuel cell vehicle is conducted, which consists of two major modules: PEM fuel cell stack module and system module, and a cooling pump. System module includes air compressor, heat exchanger, humidifier and the cooling loop. The analysis is completed using a PEM fuel cell performance model developed by two of the authors [11]. Moreover, a parametric study is conducted to investigate the effect of operating conditions on the performance of the system.

2. Thermodynamic analysis

2.1. Exergetic aspects

Exergy method of analyzing energy systems integrates the first and second law of thermodynamics and reference environmental conditions. Exergy is defined as the maximum amount of work which can be obtained from a system or a flow of matter when it is brought reversibly to equilibrium with the reference environment. Every substance or system not in equilibrium with its reference environment has some quantity of exergy, while a substance or system in equilibrium with its reference environment has no exergy since it has no ability to cause any change with respect to its reference environment. The exergy consumption during a process is proportional to the entropy production due to irreversibilities. It is a useful tool for furthering the goal of more efficient energy use, as it enables the determination of the location,

type and true magnitude of energy wastes and losses in a system [3].

Exergy of a stream of matter can be divided into different components. In the absence of nuclear, magnetism, electricity and surface tension effects, the specific total exergy is the sum of:

$$ex = ex_{\text{ke}} + ex_{\text{pe}} + ex_{\text{tm}} + ex_{\text{ch}} \tag{1}$$

where ex_{ke}, ex_{pe}, ex_{tm} and ex_{ch} are the kinetic exergy, potential exergy, thermomechanical exergy and chemical exergy, respectively. Since the changes in the kinetic and gravitational potential energies are considered to be negligible in the present study, physical exergy, which is the sum of kinetic, potential and thermomechanical exergies, reduces to thermomechanical exergy only.

The specific thermomechanical exergy at a given state is defined as follows:

$$ex_{\text{tm}} = (h - h_0) - T_0(s - s_0) \tag{2}$$

where h and s refer to specific enthalpy and entropy, respectively, at a given state. The subscript 0 represents the conditions of the reference environment (restricted).

The chemical exergy is a result of compositional imbalance between a substance and its reference environment. On a molar basis, the specific chemical exergy of a substance can be written as follows:

$$ex_{\text{ch}} = \sum_j x_j(\mu_{j0} - \mu_{j00}) \tag{3}$$

where x_j is the mole fraction of the species j in the flow, μ_{j0} is the chemical potential of species j in the flow evaluated at T_0 and P_0 and μ_{j00} is the chemical potential of species j in the flow evaluated in the reference environment (unrestricted).

2.2. The reference environment

Exergy analysis cannot be performed without defining the reference environment. Moreover, in dealing with reacting systems, two forms of equilibrium has to be defined, the environmental (restricted) state and the dead (unrestricted) state. The environmental state is a restricted equilibrium where the conditions of mechanical (P) and thermal (T) are satisfied. The dead state is an unrestricted equilibrium where the conditions of mechanical (P), thermal (T) and chemical potential (μ) are satisfied.

In the present study, restricted dead state is defined as STP condition (298 K and 1 atm), whereas the unrestricted dead state is defined (Table 1) as the composition of wet atmospheric air with relative humidity of 57.5%, which can be taken as a typical annual average [8].

2.3. Fuel cell power system

The PEM fuel cell power system considered in the present study is based on Ballard's fuel cell engine for light-duty vehicles and is shown in Fig. 1. The power system consists of two modules: the PEM fuel cell stack module and system module, and a cooling pump. The main components of the system module are air compressor, heat exchanger, humidifier and the cooling loop.

The PEM fuel cell stack module is the heart of the power system where pressurized, humidified air and hydrogen are supplied from the system module. This is the place where electrical power is produced through electrochemical reaction of hydrogen and oxygen as follows:

$$\text{H}_{2(g)} + \frac{1}{2}\text{O}_{2(g)} \Longrightarrow \text{H}_2\text{O}_{(l)} + \text{electrical power} + \text{waste heat} \tag{4}$$

Here, the waste heat produced in the stack module is removed through the cooling loop.

The air compressor component of the system module provides pressurized oxygen in the form of air, to the stack. The pressurized air is cooled down in a heat exchanger and humidified in a humidifier before being fed to the stack. Similarly, compressed hydrogen stored on-board is humidified in a humidifier before feeding to the stack. Humidification of inlet streams is necessary to prevent dehydration of the membranes in the fuel cell stack. Not all the hydrogen supplied to the fuel cell is consumed by the fuel cell stack, and therefore the unreacted hydrogen leaving the stack is recirculated.

The purpose of the cooling loop is to remove the heat produced by the exothermic reaction of hydrogen and oxygen. The cooling loop consists of a radiator, cooling pump, radiator fan. The cooling pump directs coolant (water/glycol) through the stack to remove the waste heat via radiator.

2.4. PEM fuel cell performance model

Here, the PEM fuel cell performance model developed by Baschuk and Li [11] is used to simulate the fuel cell stack. The model predicts the voltage of a single cell at any specified operating conditions. The voltage of the entire stack is then obtained by multiplying the single cell potential with the number of cells in the stack. The output voltage of a fuel cell can be represented as

$$E(I) = E_r - E_{\text{irr}} \tag{5}$$

where E_r is the reversible voltage of the cell and E_{irr} is the irreversible voltage loss or overpotential due to catalyst lay-

Table 1
Mole fractions and chemical exergy of the components at dead state

Component, i	N_2	O_2	H_2O	CO_2	Ar
Mole fraction, $x_{00,i}$	0.775	0.206	0.018	0.0003	0.0007
Chemical exergy $ex_{ch,i}$ [J·mole^{-1}]	631.51	3914.26	9953.35	20108.5	17998.14

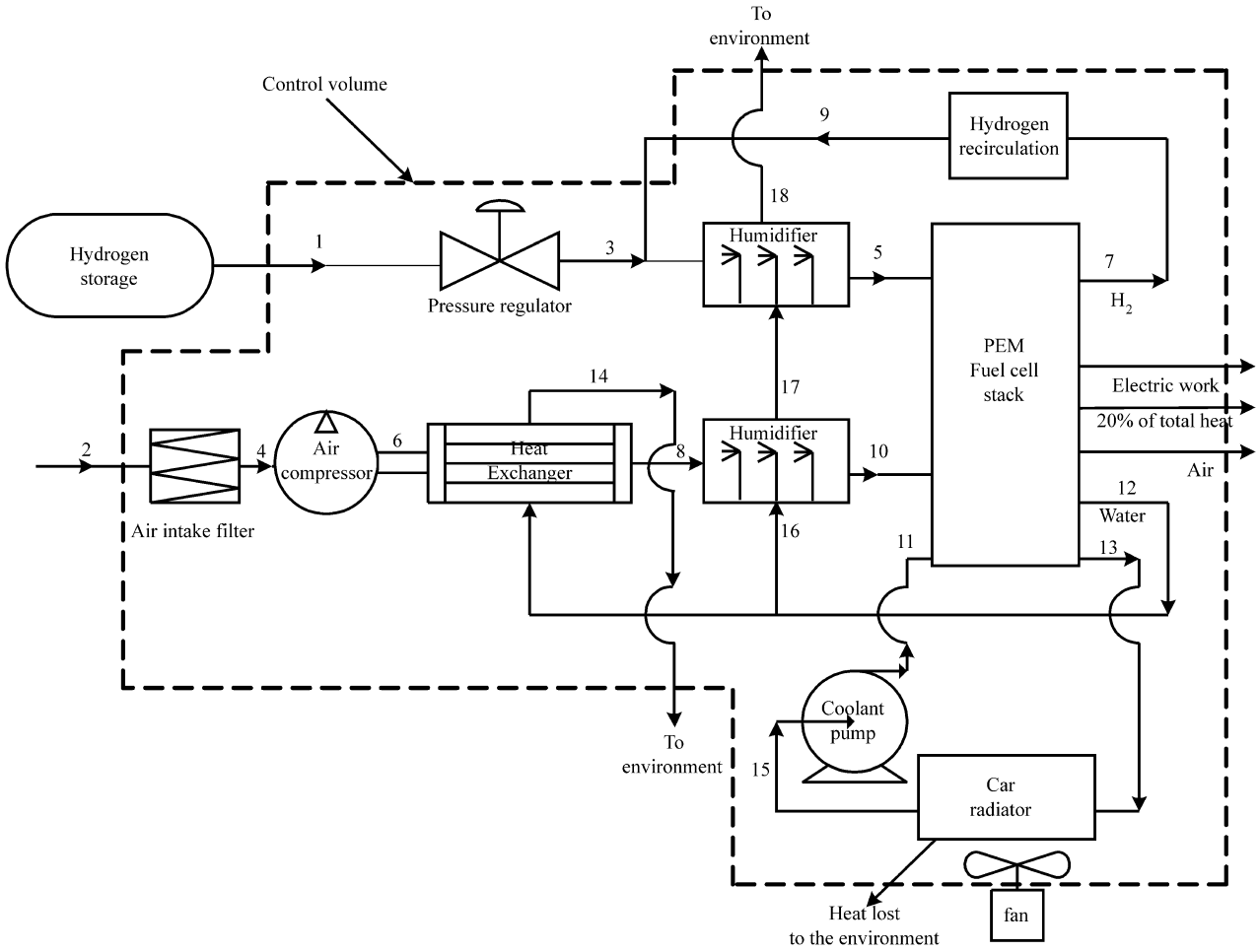

Fig. 1. Schematic of the fuel cell power system (adapted from Ballard [12]).

ers, electron migration in the bipolar plates and electrode backing, and proton migration in the polymer electrolyte membrane.

2.4.1. Reversible cell voltage (E_r)

The reversible cell voltage is the cell potential obtained at thermodynamic reversible condition. It is given by the following expression:

$$E_r = 1.229 + 0.85 \times 10^{-3}(T - 295.15) + 4.31 \times 10^{-5} T \ln\left[\left(\frac{C_{H_2}}{22.22}\right)\left(\frac{C_{O_2}}{7.033}\right)^{1/2}\right] \quad (6)$$

2.4.2. Irreversible cell voltage loss or overpotential (E_{irr})

Irreversible cell voltage loss or overpotential is composed of activation overpotential (η_{act}) due to catalyst layers, ohmic overpotential (η_{ohmic}) due to electron migration in the bipolar plates and electrode backing, and proton migration in the polymer electrolyte membrane, and concentration overpotential (η_{con}) due to the mass transfer limitations at higher current densities.

$$E_{irr} = \eta_{act} + \eta_{ohmic} + \eta_{con} \quad (7)$$

2.4.3. Activation overpotential (η_{act})

Activation overpotential is due to the catalyst layers. It takes into account the electrochemical kinetics, and electron and proton migration, and is composed of both the anode and cathode catalyst layer activation overpotentials:

$$\eta_{act} = \eta^a_{act} + \eta^c_{act} \quad (8)$$

where η^a_{act} and η^c_{act} are the activation overpotentials in the anode and cathode catalysts layers, respectively.

2.4.4. Ohmic overpotential (η_{ohmic})

The ohmic overpotential is given by the following expression:

$$\eta_{ohmic} = \eta^a_{bp} + \eta^c_{bp} + \eta^a_e + \eta^c_e + \eta_m \quad (9)$$

where η^a_{bp} and η^c_{bp} are the ohmic losses of the anode and cathode bipolar plates, respectively. The ohmic losses of the anode and cathode electrode backing layers are denoted by η^a_e and η^c_e. The overpotential due to the polymer electrolyte membrane is η_m. The detailed descriptions and expressions for these overpotentials can be found elsewhere [11].

2.4.5. Concentration overpotential (η_{con})

It is due to mass transfer limitations at higher current densities, and is composed of both the anode and cathode concentration overpotentials:

$$\eta_{con} = \eta^a_{con} + \eta^c_{con} \tag{10}$$

where η^a_{con} and η^c_{con} are the anode and cathode concentration overpotential, respectively

2.4.6. Stack power ($\dot{W}_{stack}$)

The power produced by a single cell is given as:

$$\dot{W}_{cell} = E(I) \times I \times A_{cell} \tag{11}$$

where I is the current density and A_{cell} is the geometric area of the cell.

The stack power is then obtained by multiplying the single cell power with number of cells in the stack, which can be written as:

$$\dot{W}_{stack} = n_{fc} \times \dot{W}_{cell} \tag{12}$$

where n_{fc} is the number of fuel cells in the stack. In the present power system, we consider 97 cells of 900 cm^2 geometric area in the stack producing net system power of 68 kW at $I = 1.15$ A·cm^{-2} and $E = 0.78$ V.

2.5. Assumptions

The assumptions considered in the analysis are as follows:

- The hydrogen storage cylinder or tank is at a constant pressure of 10 bar and temperature of 298 K.
- Isentropic efficiencies of compressor, cooling pump and radiator fan are assumed to be 70%.
- 20% of the total heat produced by the fuel cell stack is assumed to be lost due to convection and radiation [9].
- The temperatures at the inlet and outlet of the coolant circulation pump are assumed to be equal.
- The environmental (restricted) state is at STP conditions, i.e., 298 K and 1 atm.
- Wet atmospheric air with the composition given in Table 1 is used as dead (unrestricted) state.

The net system power produced by the fuel cell power system is obtained by deducting the parasitic loads from the gross stack power. For the present system, net system power becomes

$$\dot{W}_{net} = \dot{W}_{stack} - \dot{W}_{ac} - \dot{W}_{cp} - \dot{W}_{rf} \tag{13}$$

where $\dot{W}_{stack}$, $\dot{W}_{ac}$, $\dot{W}_{cp}$ and $\dot{W}_{rf}$ denotes stack power, power input to air compressor, cooling pump and radiator fan, respectively.

The governing thermodynamic first and second law equations are combined for the system as well as for individual components to obtain the exergy balance equation for the system and its components. The exergy balance equation for the system and energy and exergy efficiencies for the system are presented below.

2.6. Overall system

The exergy balance equation for the overall system can be written as:

$$\begin{aligned}\dot{N}_1 ex_1 + \dot{N}_2 ex_2 + \dot{N}_9 ex_9 - \dot{N}_{air} ex_{air} - \dot{N}_{14} ex_{14} - \dot{N}_{18} ex_{18} \\ - \dot{W}_{net} - \left(1 - \frac{T_0}{T_{stack}}\right)(0.2 \times \dot{Q}_{stack}) \\ - \left(1 - \frac{T_0}{T_{radiator}}\right)\dot{Q}_{radiator} - \dot{I}_{system} = 0\end{aligned} \tag{14}$$

where subscripts 1, 2, 14, and 18 stand for the states of the system shown in Fig. 1. $\dot{Q}_{stack}$ and $\dot{Q}_{radiator}$ are the rate of heat produced by the stack and rate of heat loss by the radiator to the environment, respectively. Also, $\dot{I}_{system}$ is the internal rate of exergy destruction or irreversibility for the overall system. It should be noted that in deriving all exergy balance equations, we assumed the kinetic and potential energies to be negligible and system as well as its components to be at steady state so that time derivatives are zero.

The energy and exergy efficiencies of the system are defined as follows:

$$\eta_{system} = \frac{\dot{W}_{net}}{\dot{N}_1 h_1 + \dot{N}_9 h_9} \tag{15}$$

$$\psi_{system} = \frac{\dot{W}_{net}}{\dot{N}_1 ex_1 + \dot{N}_9 ex_9} \tag{16}$$

3. Results and discussion

The analysis presented above is integrated with the fuel cell performance model developed by Baschuk and Li [11], and applied to the system with the fuel cell stack operating at varying temperatures, pressures and air stoichiometric ratios. The base-case operating conditions of the system are listed in Table 2.

The variation of net system and gross stack power with current density at base-case operating conditions is shown in Fig. 2. At a current density of 1.15 A·cm^{-2}, the net power produced by the system is around 68 kW. It can be observed from the figure that, with the increase of current density in other words, the external load, the difference between the gross stack power and the net system power increases, which is due to the increase in parasitic loads with the increase of external load.

Table 2
Base-case operating conditions

T (°C)	80
P (atm)	3
S_{fuel}	1.1
S_{air}	2.0

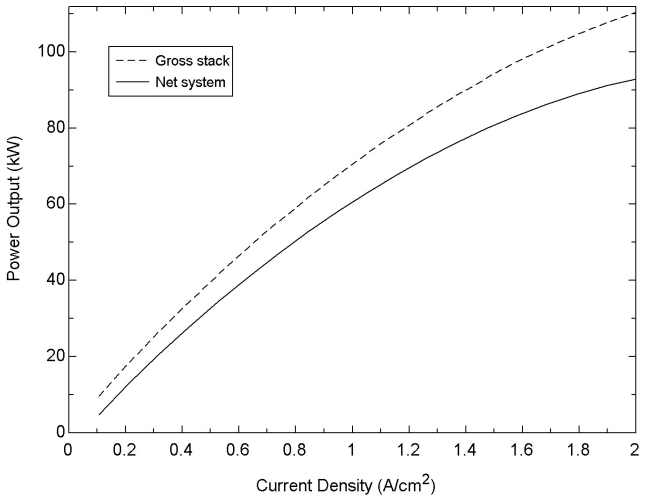

Fig. 2. Variation of power output with current density at base-case operating conditions.

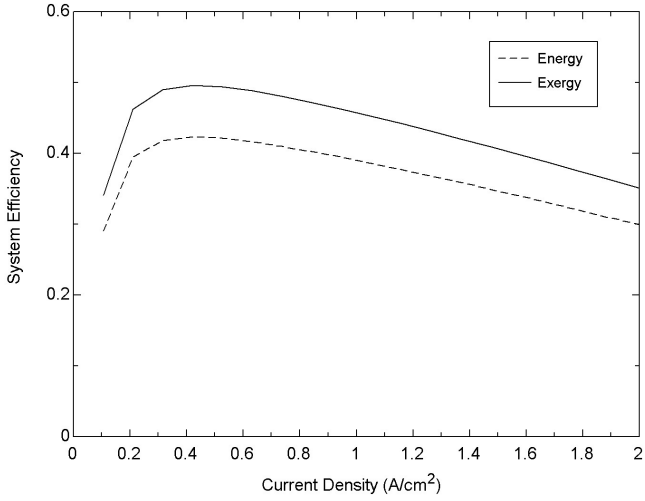

Fig. 3. Variation of system efficiencies with current density at base-case operating conditions.

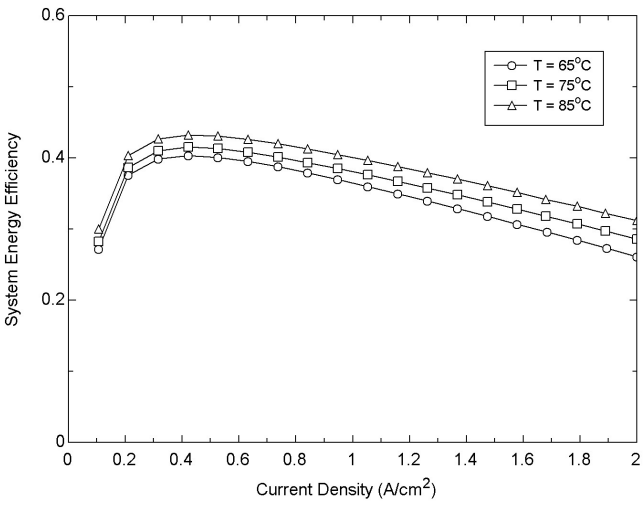

Fig. 4. Variation of system energy efficiency at different operating temperatures of fuel cell stack.

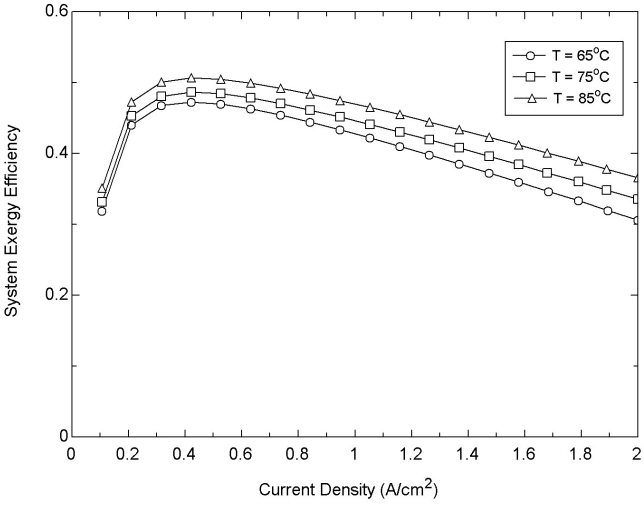

Fig. 5. Variation of system energy efficiency at different operating temperatures of fuel cell stack.

The variation of system energy and exergy efficiencies with current density at base-case operating conditions listed in Table 2 is shown in Fig. 3. The maximum system energy and exergy efficiencies are obtained as 42.32 and 49.59% respectively, at a current density of 0.42 A·cm^{-2}. The system energy and exergy efficiencies at a typical cell voltage of 0.78 V and current density of 1.15 A·cm^{-2} are found to be 37.72 and 44.20% respectively. From the figure, it can be seen that both system energy and exergy efficiencies initially increases at lower current densities reaching their peaks and finally decreases with the increase of current density. Since at lower current densities, the molar flow rate of fuel consumed by the stack is less and the power required by the auxiliary devices is low, both energy and exergy efficiencies increases until reaches their threshold values at a current density of 0.42 A·cm^{-2} and finally decreases with the increase of current density, which is due to the increase in parasitic load and molar consumption of fuel. Exergy efficiencies are higher than energy efficiency, which is due to lower exergy values at states 1 and 9 corresponding to the enthalpy values.

Figs. 4 and 5 show the energy and exergy efficiencies of the system at different operating temperatures of the fuel cell stack. The operating pressure was set as 3 atm, and air and fuel stoichiometries were kept constant at 1.1 and 2.0, respectively. It can be seen that both energy and exergy efficiencies of the system increase with the increase of temperature. This is in fact due to the decrease in irreversible losses (irreversibility) of the fuel cell stack with the increase of temperature, which in turn reduces the irreversibility of the system and hence results in increase of both energy and exergy efficiencies.

Figs. 6 and 7 show the variation of energy and exergy efficiencies of the system with current densities at different operating pressures of the stack. The operating temperature was 80 °C and air and fuel stoichiometries were set as 1.1

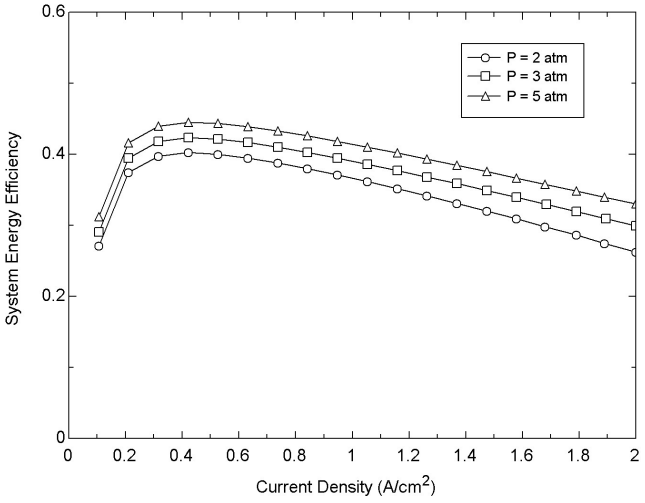

Fig. 6. Variation of system exergy efficiency at different operating pressures of fuel cell stack.

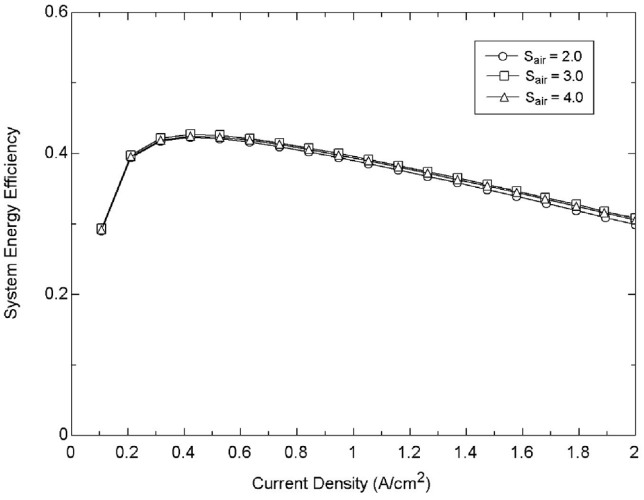

Fig. 8. Variation of system energy efficiency at different air stoichiometries of fuel cell stack.

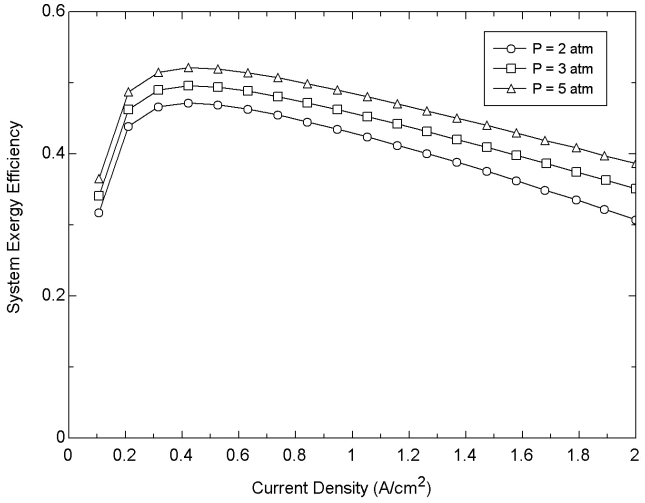

Fig. 7. Variation of system exergy efficiency at different operating pressures of fuel cell stack.

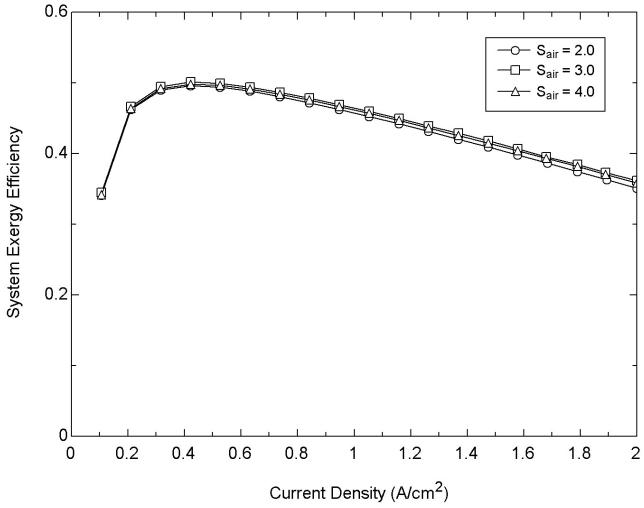

Fig. 9. Variation of system exergy efficiency at different air stoichiometries of fuel cell stack.

and 2.0, respectively. With the increase of pressure, both the energy and exergy efficiencies of the system increases. This is due to significant increase in the gross stack power as a result of decrease in irreversible losses, especially anode and cathode overpotentials, with the increase of pressure. With the increase of pressure, concentration of the reactants at the reaction sites increases, as a result the irreversible losses in the form of anode and cathode overpotentials decreases, which in turn enhances the performance of the fuel cell stack. Although, high pressure operation requires pressurization of inlet streams, which means more parasitic load in the form of power input to the compressor, but the net power produced by the system increases with the increase of pressure. Therefore, energy and exergy efficiencies of the system increase with the increase of pressure.

The variations of energy and exergy efficiencies of the system at different air stoichiometries are shown in Figs. 8 and 9. The operating temperature and pressure were set as 80 °C and 3 atm with a fuel stoichiometry of 1.1. From the figures, it can be observed there is no appreciable increase in energy and exergy efficiencies with the increase of stoichiometry of air. With the increase of air stoichiometry, molar flow rate of air increases resulting in the decrease of cathode overpotential and hence gross power produced by the stack increases. Although the gross power produced by the stack increases with the increase of air stoichiometry, but the increase in net power produced by system is not significant. Increasing the air stoichiometry from 3.0 to 4.0 has almost no increase in net power produced by the system. This is again due to increase in parasitic load which is offsetting the increase in gross stack power with air stoichiometry, resulting no significant increase in energy and exergy efficiencies with increase in air stoichiometry.

Fig. 10 shows the exergy flow diagram of the system at a particular operating condition. The bold values inside each component of the system denote the irreversibility rate. The

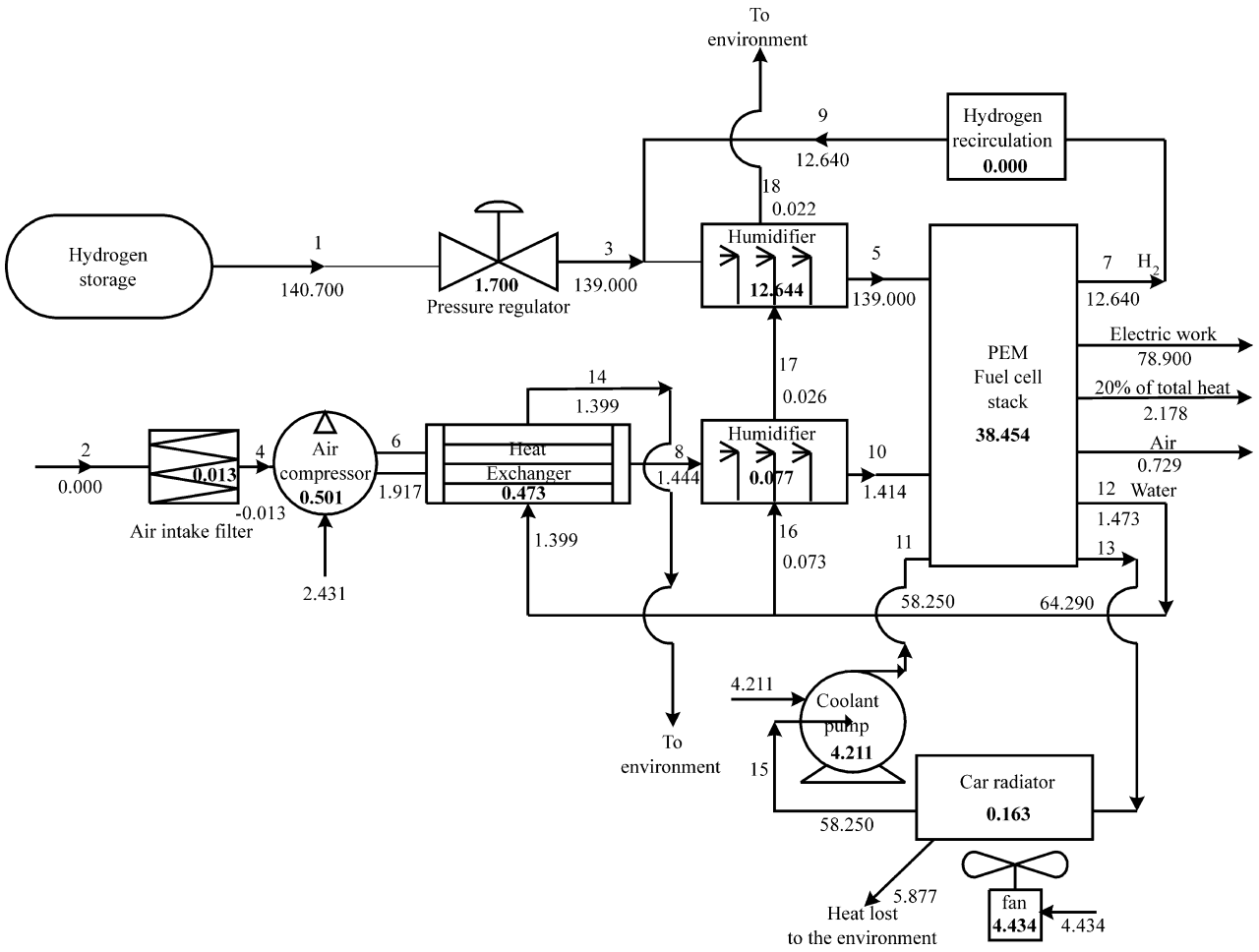

Fig. 10. Exergy flow diagram of the system at base-case operating conditions, $I = 0.938$ A·cm^{-2} and $V = 0.466$ V. Bold value in each component denotes irreversibility rate. All units are in kW.

system energy and exergy efficiencies are found to be 37.72 and 44.20% respectively. The largest irreversibility rate was found in fuel cell stack. The other major irreversibility rate was found in fuel humidifier, where hydrogen from the storage cylinder and exhaust hydrogen not utilized in the fuel cell stack are mixed and humidified before being fed into the stack. The performance of the system can be enhanced by minimizing the irreversibility rate in the fuel cell stack, which in turn reduces the cost and helps in commercialization of fuel cell power system in transportation applications.

4. Conclusions

A thermodynamic modeling based on energy and exergy analysis of a PEM fuel cell power system for light-duty vehicle has been carried out. In addition, a parametric study is conducted to examine the effect of varying operating conditions on the energy and exergy efficiencies of the system. It was found that, with the increase of external load (current density), the difference between the gross stack power and net system power increases as a result of increase in parasitic loads. Both energy and exergy efficiencies of the system increase with the increase of stack operating temperature. Although the high pressure operation increases the parasitic load in the form of power input to the compressor, but the net power produced by the system increases with the increase of pressure, which results in increase of energy and exergy efficiencies of the system with pressure. No appreciable increase in energy and exergy efficiencies was found with the increase of air stoichiometry. The largest irreversibility rate takes place in fuel cell stack. Thus, minimizing the irreversibility rates in the fuel cell stack results in enhancing the performance of the system, which in turn reduces the cost and helps in commercialization of fuel cell power system for transportation applications.

Acknowledgements

The financial support of the AUTO 21 Network of Centres of Excellence (NCE) under the Project Number D07-DFC is gratefully acknowledged. The Project is supported by the Auto 21 NCE, NRC Institute for Fuel Cell Innovation, PalCan Fuel Cells Ltd., and Hydrogenics Corporation.

References

[1] T. Ralph, G. Hards, J. Keating, S. Campbell, D. Wilkinson, M. Davis, J. St-Pierre, M. Johnson, Low cost electrodes for proton exchange membrane fuel cells performance in single cells and Ballard stacks, J. Electrochem. Soc. 144 (11) (1997) 3845–3857.

[2] C.L. Haynes, W.J. Wepfer, Enhancing the performance evaluation and process design of a commercial-grade solid oxide fuel cell via exergy concepts, ASME J. Energy Resourc. Technol. 124 (2002) 95–104.

[3] I. Dincer, Technical, environmental and exergetic aspects of hydrogen energy systems, Internat. J. Hydrogen Energy 27 (2002) 265–285.

[4] M.A. Rosen, Comparison based on energy and exergy analyses of generation devices, Internat. J. Hydrogen Energy 15 (4) (1990) 267–274.

[5] S.P. Harvey, H.J. Richter, Gas turbine cycles with solid oxide fuel cells; Part II: A detailed study of a gas turbine cycle with an integrated internal reforming solid oxide fuel cell technology, ASME J. Energy Resourc. Technol. 116 (1994) 312–318.

[6] K.W. Bedringas, I.S. Erstesvag, S. Byggstoyl, B.F. Magnussen, Exergy analysis of solid-oxide fuel cell (SOFC) systems, Energy 22 (4) (1997) 403–412.

[7] S.H. Chan, C.F. Low, O.L. Ding, Energy and exergy analysis of simple solid-oxide fuel cell (SOFC) power systems, J. Power Sources 103 (2002) 188–200.

[8] M.M. Hussain, J.J. Baschuk, X. Li, I. Dincer, Thermodynamic modeling of a PEM fuel cell power system for transportation applications, Presented at the Hydrogen and Fuel Cell Conference, 25–28 September 2004, Toronto, Canada, 2004.

[9] R. Cownden, M. Nahon, M.A. Rosen, Exergy analysis of a fuel cell power system for transportation applications, Exergy Internat. J. 1 (2) (2001) 112–121.

[10] A. Kazim, Exergy analysis of a PEM fuel cell at variable operating conditions, Energy Convers. Management 45 (2004) 1949–1961.

[11] J.J. Baschuk, X. Li, Mathematical model of a PEM fuel cell incorporating CO poisoning and O_2 (air) bleeding, Internat. J. Global Energy Issues 20 (3) (2003) 245–276.

[12] Ballard Power Systems Web page HY-80 fuel cell engine brochure, Extracted from http://www.ballard.com/be_a_customer/transportation/fuel_cell_engines/light-duty_fuel_cell_engines, 2004.